biomass

MDPI

Article

Valorization of *Hordeum vulgare* Residues into Activated Carbon for Paracetamol Removal from Water

Astrid Guadalupe Cortes-Cruz [1], Carlos Javier Durán-Valle [2], Claudia Romo-Gómez [1,*], Cesar Camacho-López [1], Otilio Arturo Acevedo-Sandoval [1], Fernando Salas-Martínez [1] and Cesar Abelardo González-Ramírez [1]

[1] Academic Area of Chemistry, Institute of Basic Sciences and Engineering, Autonomous University of the State of Hidalgo, Mineral de la Reforma 42184, Hidalgo, Mexico; co483027@uaeh.edu.mx (A.G.C.-C.); cesar_camacho@uaeh.edu.mx (C.C.-L.); acevedo@uaeh.edu.mx (O.A.A.-S.); fernando_salas@uaeh.edu.mx (F.S.-M.); cramirez@uaeh.edu.mx (C.A.G.-R.)
[2] Department of Organic and Inorganic Chemistry, University of Extremadura, Avenida de Elvas Avenue, 06006 Badajoz, Spain; carlosdv@unex.es
* Correspondence: claudiar@uaeh.edu.mx

Abstract

The presence of pharmaceutical compounds in aquatic systems represents a growing concern due to their persistence and potential adverse effects on ecosystems and human health. In this study, activated carbon obtained from *Hordeum vulgare* residues was developed and evaluated for the removal of paracetamol from aqueous solutions. The adsorbents were prepared through carbonization followed by physical activation with CO_2 at 800 °C. Their textural and chemical properties were characterized using BET, FTIR, SEM-EDX, and Boehm titration. The activation process significantly increased the surface area (up to 520 m^2 g^{-1}) and promoted the formation of a micro-mesoporous structure. Adsorption experiments were conducted at pH values of 5–7 and temperatures of 30–40 °C, using an adsorbent dosage of 1 g L^{-1} and initial concentrations ranging from 100 to 500 mg L^{-1}. The highest experimental adsorption capacity (*Qe*) (363.84 mg g^{-1}) was obtained at pH 5 and 40 °C, with a removal efficiency of 68.81%. This value exceeded the adsorption capacity reported for activated carbon derived from jatoba fruits and Merck activated carbon by 8.81% and 21.91%, respectively. Nevertheless, neither pH (p = 0.629) nor temperature (p = 0.681) exerted a statistically significant effect on adsorption capacity. The equilibrium data were better fitted by the Freundlich model (R^2 > 0.93), indicating a heterogeneous surface and multilayer adsorption. These results demonstrate that activated carbon derived from *Hordeum vulgare* is an efficient and sustainable adsorbent for the removal of emerging contaminants from water, highlighting its potential for biomass valorization.

Keywords: activated carbon; *Hordeum vulgare*; paracetamol; adsorption; biomass valorization; emerging contaminant

Check for updates

Received: 30 July 2026
Revised: 14 September 2026
Accepted: 30 September 2026
Published: 5 October 2026

Copyright: © 2026 by the authors. Licensee MDPI, Basel, Switzerland. This article is an open access article distributed under the terms and conditions of the Creative Commons Attribution (CC BY) license.

1. Introduction

The increasing occurrence of emerging contaminants in aquatic systems has become a growing environmental concern due to their persistence, continuous release, and potential adverse effects on aquatic ecosystems and human health [1]. Among these are emerging contaminants, which include personal care products, surfactants, refractory compounds, and pharmaceuticals, among many others [1]. Pharmaceutical products are organic compounds used to treat various diseases in humans and animals [2]. Therefore, they

have attracted considerable attention due to their persistence, bioactivity, and incomplete removal in conventional wastewater treatment systems.

Non-steroidal anti-inflammatory drugs (NSAIDs) are among the most frequently detected pharmaceuticals in the environment. These medications are commonly available over the counter and are widely used as anti-inflammatory and antipyretic agents [3]. In 2024, 78 pharmaceutical compounds were detected in the Llobregat and Besòs rivers [4]. Among the quantified analytes, naproxen (355 ng L^{-1}), ibuprofen (205 ng L^{-1}), diclofenac (188 ng L^{-1}), and acetaminophen (564 ng L^{-1}) were the most prominent. In Mexico, 118 pharmaceutical compounds have been reported in wastewater effluents and groundwater in the Mezquital Valley region, including trace concentrations (ng L^{-1}) of paracetamol (67,200), naproxen (18,600), and ibuprofen (5190), among others [5].

Paracetamol (APAP) is a non-steroidal anti-inflammatory drug (NSAID) and one of the most common and persistent molecules detected in water effluents due to its molecular stability, solubility, and widespread consumption. According to the literature, approximately 1–4% of the administered dose is excreted unchanged, while the majority is metabolized [6,7]. The presence of APAP has been reported at concentrations of 65, 15, 2, and 15.7 μg L^{-1} in waters from the River Tyne in England, Nairobi in Kenya, the Leine River in Germany, and Dahan in Taiwan, respectively [8–11]. In France, the United States, and Germany, paracetamol has also been detected in drinking water at trace concentrations of 0.045, 0.02, and 0.21 μg L^{-1}, respectively [12–14].

APAP has been reported to produce endocrine-disrupting because it alters the reproductive and growth cycles of aquatic fauna [15]. In addition, exposure to paracetamol has been associated with reduced heart rate, spinal abnormalities, and oxidative stress in aquatic species such as zebrafish (*Danio rerio*) and common carp (*Cyprinus carpio*) [16,17]. In humans, APAP exposure may cause hepatotoxicity and neurological damage in children, and prenatal exposure has been linked to the development of attention deficit disorders, hyperactivity, and autism spectrum disorders [18]. Currently, conventional water treatment processes have proven inefficient for removing this type of contaminant due to its physicochemical properties [19]. Therefore, alternative technologies such as membrane filtration, advanced oxidation processes, and adsorption have been extensively investigated [20]. Among these technologies, adsorption is a versatile, easy-to-operate unit process that captures contaminant molecules onto surfaces of porous materials [21]. In particular, activated carbons stand out as highly effective adsorbents for the removal of organic contaminants.

In recent years, biomass-derived activated carbons have attracted significant attention within the circular economy framework due to their low cost and the valorization of agro-industrial residues [22]. However, the inadequate management of these residues represents an environmental concern. In Mexico, approximately 0.87 million t of barley straw are generated annually, providing a substantial source of lignocellulosic biomass with potential for valorization into value-added materials [23]. In this context, valorizing lignocellulosic residues for the production of adsorbent materials represents a sustainable strategy that mitigates their environmental impact while simultaneously generating high value-added materials. Although previous studies have demonstrated that both pore structure and surface chemistry influence the adsorption of pharmaceuticals onto activated carbons, these properties may vary considerably depending on the precursor material, activation method, and characteristics of the target contaminant. In particular, limited information is available on how CO_2 physical activation of *Hordeum vulgare*-derived carbon affects its textural properties and how these properties influence paracetamol adsorption.

Therefore, the present study aims to develop activated carbon from *Hordeum vulgare* residues through CO_2 physical activation and evaluate its performance for paracetamol removal from aqueous solutions. This activation route provides a more environmentally

benign alternative to conventional chemical activation by reducing the use of corrosive or hazardous activating agents and the generation of associated chemical waste. The novelty of this work lies in evaluating how the textural and surface properties of CO_2-activated *Hordeum vulgare*-derived carbon influence its paracetamol adsorption behavior, an aspect that has been less explored in barley-derived adsorbents.

2. Materials and Methods

2.1. Reagents

Barley straw (*Hordeum vulgare*) was collected as an agricultural residue after harvesting in San Agustín Tlaxiaca, Hidalgo, México. Paracetamol (purity > 98%) was purchased from Sigma-Aldrich (St. Louis, MO, USA). Reagents, including NaOH (Reactivos Química Meyer, Mexico City, Mexico), $NaHCO_3$ (J.T. Baker, Phillipsburg, NJ, USA), HCl (Riedel-de Haën, Seelze, Germany), Na_2CO_3 (Reactivos Química Meyer, Mexico), NaCl (Reactivos Química Meyer, Mexico), and CH_3COOH (J.T. Baker, USA), were of analytical grade (purity $\geq$ 99.9%). Acetonitrile (HPLC grade, $\geq$99.9%) was supplied by Honeywell (Charlotte, NC, USA). All solutions were prepared using deionized water.

2.2. Preparation of Charcoal

Barley straw (*Hordeum vulgare*), a residue from barley grain production for beer brewing, was used as the precursor material. After collection, the *Hordeum vulgare* residues were transported to the laboratory, where they were washed under running tap water to remove soil and other foreign materials. The residues were then soaked in water for 12 h, rinsed with deionized water, and allowed to dry at room temperature. Once air-dried, the barley straw was cut into smaller pieces to facilitate its placement on trays and subsequently oven-dried at 105 °C for 24 h to ensure complete drying. Finally, the dried material was ground to obtain a particle size of 1.4 mm.

Two types of carbon materials were prepared: a non-activated carbon (char) and an activated carbon. For the carbonization process, 30 g of biomass were treated in a tubular furnace (Carbolite Gero, Hope, Derbyshire, UK) at 800 °C for 3 h under an N_2 flow of 400 mL min^{-1} and a heating rate of 10 °C min^{-1}. The carbonization yield was calculated using the following equation, ten independent batches were prepared:

$$Y_C = \frac{m_{biomass}}{m_{char}} * 100\% \quad (1)$$

The resulting material was repeatedly washed with deionized water at 90 °C until the washing water reached a neutral pH (7.00 $\pm$ 0.05). The material was then dried at 70 °C for 24 h.

2.3. Activation

Physical activation was carried out using CO_2 (400 mL min^{-1}) at 800 °C for 2 h and heating rate of 10 °C min^{-1}. The activation yield was determined according to the following equation, a total of 10 batches of activated carbon were produced under the same experimental conditions:

$$Y_A = \frac{m_{activatedcarbon}}{m_{char}} * 100\% \quad (2)$$

The activated carbon was subsequently washed and dried under the same conditions previously described.

2.4. Surface Characterization of Adsorbents

The textural properties were determined from N_2 adsorption–desorption isotherms at 77 K using an Autosorb iQ-C analyzer (Quantachrome Instruments, Boynton Beach, FL, USA).

Prior to analysis, the samples were degassed at 120 °C for 24 h. The specific surface area was calculated using the Brunauer–Emmett–Teller (BET) method, while the micropore volume was estimated using the Dubinin–Radushkevich (DR) model. The mesopore volume and pore size distribution were determined using Density Functional Theory (DFT) with the carbon slit-pore equilibrium model implemented in ASiQwin software version 4.0 (Quantachrome Instruments, Boynton Beach, FL, USA). The morphology and elemental composition of the carbonaceous materials were analyzed by scanning electron microscopy (SEM) using a Quanta 3D FEG microscope (FEI Company, Hillsboro, OR, USA) operated under high-vacuum conditions. Secondary electron (ETD, FEI Company, Hillsboro, OR, USA) and backscattered electron (BSED, FEI Company, Hillsboro, OR, USA) detectors were used for morphological and compositional imaging, respectively, while energy-dispersive X-ray spectroscopy (EDX) was employed for elemental analysis.

2.5. Functional Group Analysis

The presence of functional groups before and after the adsorption experiments was analyzed by Fourier-transform infrared spectroscopy (FTIR) within the range of 4000–400 cm^{-1}. FTIR analysis was used as a qualitative and complementary characterization technique to identify changes in surface functional groups; therefore, quantitative band deconvolution was not performed. Additionally, Boehm titration was performed to quantify the oxygen-containing functional groups [24]. For this purpose, 0.20 g of char and activated carbon, separately, were mixed with 20 mL of 0.1 M Na_2CO_3, NaOH, $NaHCO_3$, and HCl solutions in flasks which were then sealed hermetically. The experiments were carried out under dark conditions at room temperature for 5 days. Subsequently, 5 mL aliquots of the Na_2CO_3, NaOH, and $NaHCO_3$ solutions were collected, filtered, supplemented with one drop of phenolphthalein, and titrated with 0.1 M HCl solution. For the HCl experiments, the same procedure was followed, but the titration was performed using 0.1 M NaOH. All experiments were carried out in triplicate [25,26]. In the conventional Boehm titration, $NaHCO_3$ is assumed to neutralize carboxylic groups, Na_2CO_3 neutralizes carboxylic and lactonic groups, and NaOH neutralizes carboxylic, lactonic, and phenolic groups. The basic surface groups are quantified by reaction with HCl [27].

2.6. Point of Zero Charge (PZC)

The point of zero charge (PZC) was determined using the pH drift method. Briefly, 0.5 g of char and 0.5 g of activated carbon were separately placed in 50 mL polypropylene conical tubes, followed by the addition of 50 mL of 0.01 M NaCl solution as the supporting electrolyte. The initial pH was adjusted to 2, 4, 6, 8, 9, and 11 using HCl or NaOH. The suspensions were then placed in an incubator shaker (LabDoctor, MIDSCI Fenton, MO, USA) at 150 rpm and 30 °C for 72 h. The equilibration time was selected based on the procedure reported by others authors [28,29]. After the equilibration period, the final pH was measured. The PZC was determined as the pH at which the initial and final pH values converged [28].

2.7. Adsorption Experiments

The initial concentrations were selected to assess the performance of the adsorbent under relatively high contaminant-loading conditions, while accounting for the sensitivity and analytical limitations of the equipment employed. Furthermore, the selected concentration range and adsorbent dosage facilitate a meaningful comparison with previously reported adsorption studies [30–32]. Batch adsorption experiments were carried out using 1 g L^{-1} of the previously prepared adsorbents (char and activated carbon) and paracetamol solutions with initial concentrations of 100, 200, 300, 400, and 500 mg L^{-1}. The experiments were conducted at initial pH values of 5, 6, and 7. The initial pH of the

paracetamol solutions was adjusted using 0.1 M HCl or NaOH solutions, as required. No buffer solution was used to avoid introducing additional ionic species that could potentially interfere with the adsorption process. The experiments were carried out at temperatures of 30 and 40 °C under constant agitation at 120 rpm for 24 h using a shaking incubator, which allowed the temperature and agitation conditions to be maintained throughout the experiments. A contact time of 24 h was selected to ensure the attainment of adsorption equilibrium, in accordance with previously reported studies on paracetamol adsorption onto activated and biomass-derived carbonaceous materials [33]. All experiments were performed in triplicate.

The residual paracetamol concentration was determined using high-performance liquid chromatography (HPLC) (Perkin Elmer Series 200, Norwalk, CT, USA) equipped with a UV–Vis detector and a CSH Fluoro-Phenyl column (Viridis, 4.6 mm × 100 mm, 5.0 µm). The detection wavelength was selected considering the analytical method reported in the literature [34] and was experimentally verified by performing a UV–Vis spectral scan. Under the analytical conditions used in this study, the maximum absorbance of paracetamol was observed at 249 nm; therefore, this wavelength was selected for its quantification The mobile phase consisted of acetonitrile/water/acetic acid (50:49:1, v/v) at a flow rate of 1 mL min^{-1}. The injection volume was 20 µL with a run time of 15 min, and all analyses were performed at room temperature. Data processing was carried out using TC Nav software version 6.3.1. Prior to analysis, all samples were filtered through a 0.45 µm nylon membrane filter. All reagents used in the chromatographic analysis were supplied by J.T. Baker (Phillipsburg, NJ, USA). Paracetamol was quantified using a nine-point calibration curve over a concentration range of 10–500 mg L^{-1}. The calibration curve was described by the equation y = 0.0054x − 0.0294, with a coefficient of determination (R^2) of 0.99929, demonstrating good linearity within the evaluated concentration range. The experimental data were fitted to the Langmuir Equation (3) and Freundlich Equation (4) isotherm models in order to describe the adsorption equilibrium.

$$Q_L = \frac{Q_{max} K_L C_e}{1 + K_L C_e} \tag{3}$$

$$Q_F = K_F C_e^{1/n} \tag{4}$$

where Q_L or Q_F is the adsorption capacity at equilibrium according to the model (mg g^{-1}), Q_{max} is the maximum adsorption capacity (mg g^{-1}), K_L is the Langmuir constant (L mg^{-1}), and C_e is the equilibrium concentration of the adsorbate in solution (mg L^{-1}). In the Freundlich model, K_F is the Freundlich constant (mg g^{-1} (mg $L^{-1})^{-1/n}$), and n is an indicator of adsorption intensity. Values of $n > 1$ indicate favorable adsorption, suggesting a high affinity between the adsorbent and the adsorbate [35]. The removal efficiency (E) was calculated using Equation (5), where Ci is the initial APAP concentration (mg L^{-1}) and Cf is the APAP concentration (mg L^{-1}) after 24 h of adsorption.

$$Efficiency\ (\%) = \frac{C_i - C_f}{C_i} * 100\% \tag{5}$$

2.8. Statistical

To evaluate statistically significant differences among the adsorption treatments, a multifactorial analysis of variance (ANOVA) was performed using the removal efficiency and adsorption capacity data obtained for the different materials (α = 0.05). The experimental factors considered were material type, pH, and temperature. Prior to ANOVA, the assumptions of normality, homogeneity of variances, and independence of observations were assessed at a significance level of α = 0.05. When significant differences among

treatment means were identified, Tukey's multiple comparison post hoc test was applied to determine which treatments differed significantly ($\alpha = 0.05$).

3. Results and Discussion

3.1. Production of Activated Carbon

The *Hordeum vulgare* biomass exhibited a carbonization yield of 36 ± 1.9%. Following carbonization, CO_2 activation resulted in a relatively high solid yield of 87 ± 0.6%, corresponding to a mass loss of approximately 13% during activation. This mass loss can be attributed to the partial gasification of the carbon matrix by CO_2, which is expected to promote pore development while retaining most of the carbonaceous framework. Thus, the relatively high activation yield suggests a moderate degree of burn-off under the applied activation conditions.

3.2. Characterization

Figure 1 shows the micrographs obtained by scanning electron microscopy (SEM). Figure 1a,b correspond to images acquired using the backscattered electron detector (BSED), which provides compositional information. In these images, regions containing elements with higher atomic numbers appear as bright (white) spots. Figure 1c,d were obtained using the secondary electron detector (ETD), which allows the analysis of surface morphology, including relief, roughness, and surface edges of carbonaceous materials. The micrographs show heterogeneous surfaces in both materials; however, the activated carbon exhibits a more developed porous structure, with better-defined pores and a greater pore volume compared to the carbonized material. This behavior is attributed to the release of volatile matter during the activation process, which promotes pore formation and enlargement [36]. Furthermore, energy-dispersive X-ray spectroscopy (EDX) analysis performed on the bright regions in Figure 1a,b revealed a high silicon (Si) content in the obtained carbons. The EDX spectra shown in Figure 1e indicate that Point 1, corresponding to a randomly selected point on the general surface, was predominantly carbon-rich, whereas Point 2, corresponding to the bright spots, exhibited a composition of 25.1 ± 0.2 wt% Si, 36.0 ± 0.3 wt% O, and 37.8 wt% C. The enrichment in Si and O indicates the presence of a Si-rich inorganic phase, which is consistent with silica-containing mineral deposits derived from the lignocellulosic precursor. Some authors mentioned that grasses such as rice and barley possess vascular bundle-type structures characterized by significant silica (SiO_2) accumulation [37].

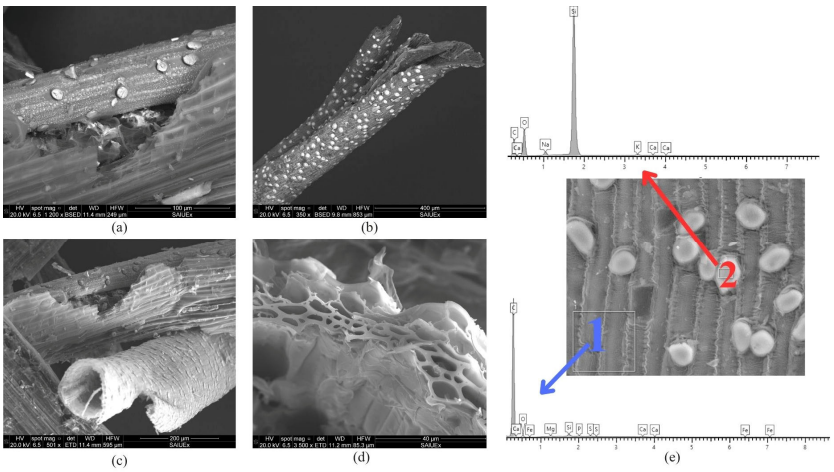


Figure 1. Scanning electron microscopy with BSED detector for (**a**) barley char and (**b**) activated carbon, and with ETD for (**c**) barley char and (**d**) activated carbon. (**e**) EDX spectrum of points 1 (general surface, blue) and 2 (bright spots, red) on the carbon surface.

Table 1 presents the results of the elemental analysis of carbons derived from *Hordeum vulgare*, in which carbon, oxygen, and silicon are the predominant elements. These results are consistent with those reported by [38], who indicate that the carbon content in this type of material typically ranges from 85 to 95 wt.%, with the remainder mainly comprising oxygen and trace amounts of other elements, such as metals and halogens. As previously mentioned, the Si content is associated with the composition of the biomass cell wall. The predominantly carbonaceous nature of the material is further supported by its elemental surface composition, in which carbon (85.66 and 88.76%) represents the major component, whereas Si (2.45 and 1.33%) constitutes only a minor fraction. Therefore, although Si containing mineral phases are present, their specific contribution to APAP adsorption cannot be independently established from the present results. Nevertheless, considering their relatively low abundance, the adsorption behavior is likely dominated by the carbonaceous matrix and its developed porous structure [39,40].

Table 1. Elemental analysis of carbon materials derived from *Hordeum vulgare*.

Material	Element (%)										
	C	O	Na	Mg	Si	P	S	Cl	K	Ca	Fe
Barley Char	85.66	8.88	0.2	0.34	2.45	0.55	0.18	0.12	0.21	0.83	0.58
Activated carbon	88.76	7.4	LOD	0.22	1.33	0.36	0.17	LOD	LOD	0.68	1.08

LOD: Below the limit of detection.

The results for the textural parameters of the adsorbents (Table 2) show that the activation process increased the specific surface area by up to 22.89 times, accompanied by a 1.88-fold increase in mesopore volume and the development of microporosity. According to the IUPAC (International Union of Pure and Applied Chemistry) classification, micropores have diameters smaller than 2 nm, mesopores range from 2 to 50 nm, and macropores are larger than 50 nm in diameter [41]. Therefore, the material can be classified as micro–mesoporous, which favors the diffusion of APAP toward the internal active sites. Such structures are characterized by the presence of well-defined diffusion channels that facilitate the transport of macromolecules, reduce mass-transfer resistance, and are thermodynamically stable [42].

Table 2. Textural parameters of carbonaceous materials derived from *Hordeum vulgare*.

Adsorbent Material	Specific Surface Area	Micropore Volume	Mesopore Volume	Macropore Volume	Total Pore Volume
	$m^2\ g^{-1}$	$cm^3\ g^{-1}$	$cm^3\ g^{-1}$	$cm^3\ g^{-1}$	$cm^3\ g^{-1}$
Barley Char	23	LOD	0.133	0.018	0.151
Activated carbon	520	0.216	0.250	0.023	0.489

LOD: Below the limit of detection, micropore volume was calculated by DR and mesopore volume by DFT.

The specific surface area obtained for the *Hordeum vulgare*-derived activated carbon (520 $m^2\ g^{-1}$) was compared with values reported for activated carbons prepared from other lignocellulosic precursors. Wazir and collaborators [36] reported a specific surface area of 443 $m^2\ g^{-1}$ for activated carbon obtained from rice residues, whereas Pietrzak [43] reported 75 $m^2\ g^{-1}$ for activated carbon derived from pine sawdust. These differences should be interpreted with caution, since the textural properties of activated carbons depend not only on the nature of the precursor but also on the carbonization and activation conditions used in each study.

Activated carbons obtained by chemical activation have also shown different textural properties. For example, surface areas reported for coconut shell carbon activated with

NaOH and palm kernel shell carbon activated with H_3PO_4 were comparable to that obtained in the present study [44,45]. However, direct comparison among these materials is limited by differences in precursor composition, activating agent, temperature, activation time, and other experimental conditions. Therefore, these literature values are presented as a general reference rather than as a direct comparison of activation efficiency. The physical activation with CO_2 used in the present study also avoids the use of chemical activating agents and the associated washing steps.

Figure 2a shows the nitrogen adsorption–desorption isotherms at 77 K. The DR analysis showed the development of microporosity after CO_2 activation, while the DFT analysis indicated an increase in mesopore volume and confirmed the micro–mesoporous pore size distribution of the activated carbon (Table 2 and Figure 2b). According to the IUPAC classification, both samples exhibit Type IVa isotherms with an H4 hysteresis loop, characteristic of mesoporous materials with slit-shaped pore features and indicating the presence of capillary condensation within the mesopore network. The carbonized sample shows a relatively low uptake in the low relative-pressure region ($p/p_0 \approx 0.05$) suggesting a limited contribution of narrow micropores. In contrast, the activated carbon exhibits a pronounced increase in N_2 uptake at low relative pressures, indicating the development of a significant microporous fraction after CO_2 activation. The hysteresis observed at intermediate-to-high relative pressures is associated with mesopore filling and confirms the development of a micro–mesoporous structure [46,47]. Studies on commercial activated carbons from coconut shell report similar trends in the adsorption branch; however, in the desorption branch, the hysteresis loop tends to close. This behavior indicates that the adsorption process is reversible [48].

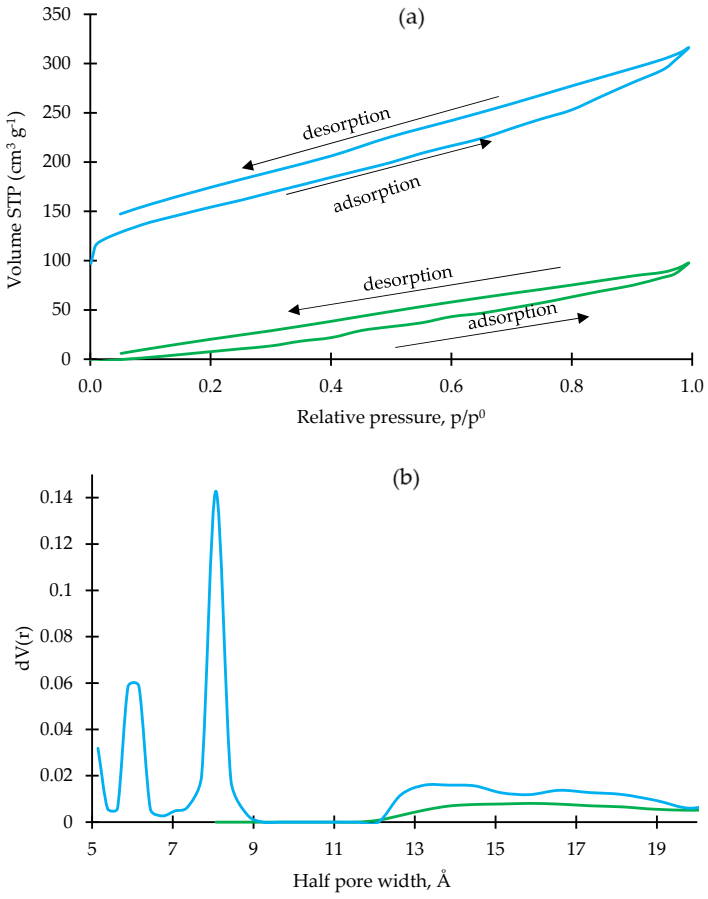


Figure 2. (**a**) N_2 adsorption-desorption isotherms at 77 K and (**b**) pore size distribution for barley char (■) and activated carbon (■).

Figure 2b shows that the physical activation of *Hordeum vulgare*-derived carbon promotes both micropore formation and an increase in mesopore volume, resulting in a micro–mesoporous structure. This feature reflects greater structural complexity and surface heterogeneity of the material [49], which facilitates the transport of larger molecules through mesopores toward active sites located within micropores [50].

Figure 3a,b present the Fourier transform infrared (FTIR) spectra of the carbonized material and the *Hordeum vulgare*-derived activated carbon prior to the adsorption process. A broad band in the 3200–3600 cm^{-1} region is observed, attributed to O–H stretching vibrations associated with phenolic groups, carboxylic acids, or adsorbed moisture [29]. In particular, the band centered at 3458 cm^{-1} decreases in intensity after the activation process, suggesting the removal of surface moisture due to thermal evaporation [51]. Likewise, the signals in the 1550–1630 cm^{-1} range are assigned to C=C stretching vibrations corresponding to aromatic structures, such as pyrone-like groups, which are characteristic of carbonaceous materials [52]. Finally, the band observed at approximately 430 cm^{-1} is associated with the O–Si–O bending mode. The presence of this inorganic fraction is not necessarily detrimental to pharmaceutical adsorption. Previous studies have shown that silica-containing phases can contribute to adsorbate uptake through hydrogen bonding involving surface silanol groups, while the carbonaceous fraction provides additional adsorption sites through hydrogen bonding, π–π interactions and pore filling [53]. Therefore, the presence of the silica phase identified in the present material is considered a secondary mineral component rather than evidence of an adverse effect on APAP adsorption.

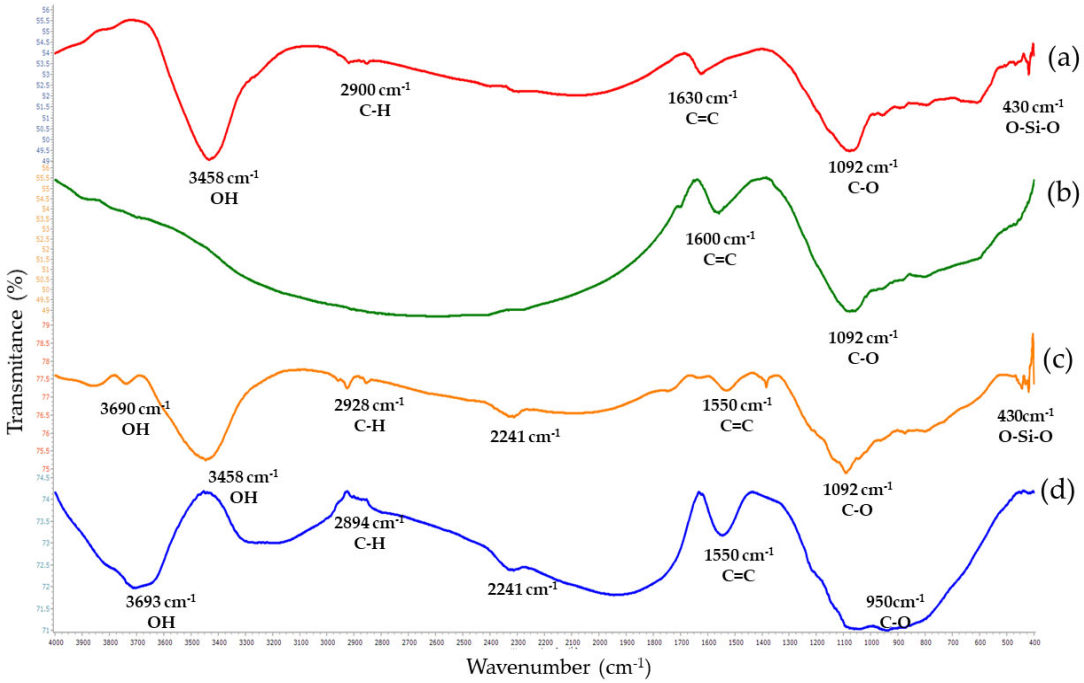


Figure 3. FTIR spectra of barley char and activated carbon (**a**,**b**) before and (**c**,**d**) after paracetamol adsorption.

Table 3 presents the point of zero charge (PZC) and the quantification of surface functional groups determined by Boehm titration. The obtained results are consistent with the FTIR analysis, confirming the presence of carboxylic groups and aromatic structures on the material surface. In particular, pyrone-type groups contribute to the basicity, which is reflected in PZC values of 7.5 and 8.0 for the activated carbon and carbonized material, respectively [54,55]. The negative values obtained for certain functional groups should not be interpreted as physically meaningful negative concentrations. Similar anomalous results

have been reported for biomass-derived carbonaceous materials and have been attributed to deviations from the ideal assumptions of the Boehm titration method, including the dissolution of inorganic components, ash, and other reactive species during the titration procedure. These matrix-related effects can alter titrant consumption and consequently lead to apparent negative values [56,57]. Therefore, in the present study, the negative values are considered non-quantifiable (ND), indicating that the corresponding functional groups could not be reliably quantified within the resolution of the method. Matrix-related interferences associated with the inorganic fraction of the *Hordeum vulgare* biomass, including its Si-containing components, may also have contributed to these results. The PZC corresponds to the pH at which the material surface has a net zero charge and, together with the acid dissociation constant (pKa) of the adsorbate (APAP), allows interpretation of the protonation state as a function of the solution pH. Specifically, when pH < PZC (adsorbent) or pH < pKa (adsorbate), protonated species predominate; otherwise, deprotonated or ionized species are favored.

Table 3. PZC and Boehm titration of *Hordeum vulgare*-derived carbon materials.

Material	PZC	Cx ($NaHCO_3$)	Py (HCl)	Ph + Cx + Lc (NaOH)	Lc + Cx (Na_2CO_3)
		mmol g^{-1}	mmol g^{-1}	mmol g^{-1}	mmol g^{-1}
Barley Char	8.0	0.9 ± 0.08	1.6 ± 0.03	−0.4 ± 0.13	−0.8 ± 0.06
Activated carbon	7.5	1.2 ± 0.03	1.7 ± 0.13	−0.4 ± 0.10	−0.7 ± 0.03

Cx: Carboxylic, Py: Pyronic, Ph: Phenolic, Lc: Lactonic.

Considering that the pKa of paracetamol is 9.38 and the PZC values of the materials are 7.5 and 8.0, within the evaluated pH range (5–7), APAP are predominantly in its neutral form, while the adsorbent surfaces are expected to be positively charged [58]. Under these conditions, electrostatic interactions are not expected to be the main adsorption mechanism, and other interactions, such as hydrogen bonding, π–π interactions, and pore filling, may contribute to APAP adsorption. Although the highest adsorption capacity was observed at pH 5, lower pH values were not evaluated in this study. Therefore, pH 5 should be considered the best condition within the investigated range rather than an absolute optimum.

The PZC values obtained for the carbonized material (8.0) and the activated carbon (7.5) fall within the typical range reported in the literature (5–9) [59]. Previous studies have reported PZC values of 8.0 for Sigma-Aldrich activated carbon [60], 6.17 for activated carbon derived from tomato [61], 5.17 for rubber fig leaves [62] and 8.74 for walnut shell-derived carbon [63]. The PZC value depends on the nature of the lignocellulosic precursor, as well as the carbonization (temperature) and activation conditions. When biomass contains carbonates or bicarbonates, these act as alkaline activating agents, promoting the formation of basic aromatic structures such as pyrone and chromene groups [64]. Likewise, inorganic salts present in the biomass can be deposited on the material surface during carbonization, thereby increasing the PZC [65].

In addition, increasing the carbonization temperature promotes the decomposition of acidic functional groups such as lactone and carboxyl groups, generating surfaces with a higher basic character [66]. This phenomenon is consistent with the results shown in Table 3, where thermal treatment at 800 °C for the preparation of the carbonaceous adsorbents favored the formation of pyrone-type basic groups, whose proportion was 1.62 and 2.27 times higher than that of carboxylic groups present in the carbonized material and the activated carbon, respectively. Another factor influencing the PZC is the activating agent, since it may decrease when acidic agents are used or increase in the presence of basic agents [67].

3.3. Adsorption Studies

Table 4 shows that the Freundlich model generally provided a better description of the experimental data, based on the combined evaluation of R^2 and RMSE values. In most experimental conditions, Freundlich exhibited higher R^2 values and lower RMSE values than Langmuir. Therefore, model selection was not based on a specific R^2 threshold, but on the overall goodness of fit. This behavior suggests that the adsorption process occurs on a heterogeneous surface and may involve multilayer adsorption. These characteristics are consistent with the surface morphology observed in the micrographs shown in Figure 1 [68,69]. Adsorption isotherms allow the evaluation of adsorbate–adsorbent affinity, the assessment of surface homogeneity or heterogeneity, and the estimation of adsorption capacity, defined as the amount of APAP retained per unit mass of adsorbent (carbon) [70]. In this context, Mabalane et al. [71] reported that the Freundlich model adequately described the adsorption behavior of APAP on activated carbon derived from plant biomass. In the present study, the activation process contributed to an approximately four-fold increase in adsorption capacity, which is mainly attributed to the 22.89-fold increase in the specific surface area of the carbonized material after CO_2 treatment. According to Tukey's multiple comparison test, the activated carbon exhibited a significantly higher mean experimental adsorption capacity (213.98 mg g^{-1}) than the non-activated carbon (59.28 mg g^{-1}), confirming the beneficial effect of CO_2 activation on the adsorption performance of the material. This improvement can be mainly attributed to the development of the porous structure and the increase in specific surface area and pore volume, which enhance the availability and accessibility of adsorption sites for APAP molecules.

Table 4. Adsorption capacity.

pH	Temperature (°C)	*Qe* (mg g^{-1})	Freundlich				Langmuir		
			K_F (mg g^{-1} (mg L^{-1})$^{-1/n}$)	*n*	R^2	RMSE	K_L (L mg^{-1})	R^2	RMSE
Barley char									
7	30	77.97 ± 1.7	1.733	1.27	0.94	3.712	0.00265	0.77	5.384
7	40	84.18 ± 1.9	1.896	1.26	0.93	3.989	0.00271	0.74	5.779
6	30	83.05 ± 1.6	2.366	1.36	0.95	3.759	0.00321	0.93	5.720
6	40	87.01 ± 1.2	2.809	1.46	0.95	2.844	0.00356	0.92	4.989
5	30	88.36 ± 0.4	2.848	1.49	0.95	2.769	0.00355	0.94	4.965
5	40	89.83 ± 0.6	3.655	1.58	0.95	2.818	0.00423	0.94	5.244
Activated carbon									
7	30	349.72 ± 2.5	12.497	1.34	0.98	5.040	0.00644	0.97	13.263
7	40	353.11 ± 1.0	13.404	1.33	0.96	7.174	0.00693	0.94	15.470
6	30	355.37 ± 1.9	13.650	1.33	0.97	7.916	0.00706	0.93	16.036
6	40	359.89 ± 1.9	13.827	1.31	0.96	9.324	0.00714	0.90	17.359
5	30	360.45 ± 0.3	15.090	1.32	0.95	11.046	0.00779	0.88	19.525
5	40	363.84 ± 0.9	15.831	1.37	0.94	12.752	0.00817	0.87	21.117

Qe: Experimental adsorption capacity, K_F: Freundlich constant, *n*: indicator of adsorption intensity, K_L: Langmuir constant, R^2: Determination coefficient, RMSE: Root Mean Square Error.

The *Hordeum vulgare*-derived activated carbon exhibits competitive performance compared to materials reported in the literature. Under similar temperature and pH conditions, its adsorption capacity (*Qe*) (Table 4) is 4.14, 1.095, and 0.95-fold higher than that of NaOH-activated carbons obtained from palm leaves (87.87 mg g^{-1}), pistachio shells (332.2 mg g^{-1}), and peanut shells (383.1 mg g^{-1}), respectively [72,73]. Overall, adsorption capacity is strongly governed by pore development, specific surface area, and the availability of active sites [74]. In this context, previous studies have evaluated materials activated using strong acidic agents, such as *Cannabis sativa*-derived carbon activated with H_3PO_4 and carbon derived from guava leaves treated with H_2SO_4, reporting adsorption capacities (Q) of 16.18 and 13.3 mg g^{-1}, respectively [69,74]. In comparison, the *Hordeum vulgare*-derived material developed in this

study exhibits values that are 22.48 to 27.36-fold higher, suggesting the strong influence of both the lignocellulosic precursor and the activation method on adsorption performance.

Similarly, Nguyen and collaborators [75] evaluated a commercial activated carbon, reporting a maximum adsorption capacity of 221 mg g^{-1} obtained from the Langmuir model. This value is 1.65-fold lower than that achieved by the *Hordeum vulgare*-derived activated carbon developed in the present study, highlighting its potential as an efficient adsorbent. These results suggest that the applied physical activation promotes the development of a micro–mesoporous structure with high accessibility to active sites, significantly enhancing adsorption performance. Consequently, the material can be considered a sustainable and efficient alternative for the removal of emerging contaminants.

Figure 4 shows the adsorption isotherms obtained for the carbonized material and the activated carbon. These results indicate that the adsorption data for both materials were better described by the Freundlich model. APAP shows higher affinity for the adsorbent at pH 5 than at pH 6 and 7, with an approximate 1.4% decrease in removal efficiency as the pH increases. This behavior is attributed to the fact that solution pH controls both the adsorbent's surface charge and the adsorbate's speciation [76]. Similar trends have been reported in the literature for APAP removal, where the removal efficiency decreases by 8–15% when the pH increases from 5 to 7, using activated carbons derived from *Cannabis sativa*, *Erythrina speciosa* and *Gundelia tournefortii* [74,77,78]. The analysis of variance showed that pH (p= 0.629) and temperature (p= 0.681) did not exhibit statistically significant effects under the evaluated conditions.

After adsorption, FTIR spectra (Figure 3c,d) show evident changes compared to the materials before adsorption (Figure 3a,b), confirming interactions between APAP and the surface of the *Hordeum vulgare*-derived activated carbon. A broad band in the 3200–3600 cm^{-1} region, associated with O–H stretching vibrations from phenolic groups, carboxylic acids, and adsorbed water [29], is observed. The band at 3458 cm^{-1} decreases after activation (Figure 3b), indicating the removal of moisture during thermal treatment [50]. In this context, the more defined bands observed in the 3690–3693 cm^{-1} region correspond to surface –OH groups with low or negligible participation in hydrogen bonding, i.e., more isolated or structurally well-defined hydroxyl groups. These groups are particularly relevant, as they exhibit greater availability for interactions with adsorbed molecules.

After the adsorption process, the shift in these bands suggests the involvement of surface –OH groups in specific interactions with APAP, where they may act as proton donors, while oxygen and nitrogen atoms in the adsorbate (APAP) function as acceptors [79]. This behavior is consistent with the formation of hydrogen bonds between the adsorbent and the adsorbate [80].

Likewise, after adsorption, an additional band was observed at approximately 2241 cm^{-1}. Based on previous FTIR assignments, bands in this region are characteristic of the stretching vibration of nitrile groups (C≡N). The characteristic amide vibrations of APAP are observed at approximately 1654 cm^{-1} (C=O stretching) and 1564 cm^{-1} (N-H bending) [81]. A weak band observed at approximately 2241 cm^{-1} after adsorption could not be unequivocally assigned to a functional group of paracetamol and was therefore not considered as direct evidence of APAP adsorption. Instead, the appearance of this band after adsorption may be associated with changes in the surface chemical environment induced by APAP adsorption.

The signals in the 1550–1630 cm^{-1} region, observed in the materials before contact with APAP (Figure 3a,b), are associated with C=C vibrations of aromatic pyrone-like structures [51]. After adsorption, these bands shift toward 1550 cm^{-1}, while C–O bands shift toward 950 cm^{-1}, suggesting π–π and n–π interactions between the adsorbate and the adsorbent surface [82].

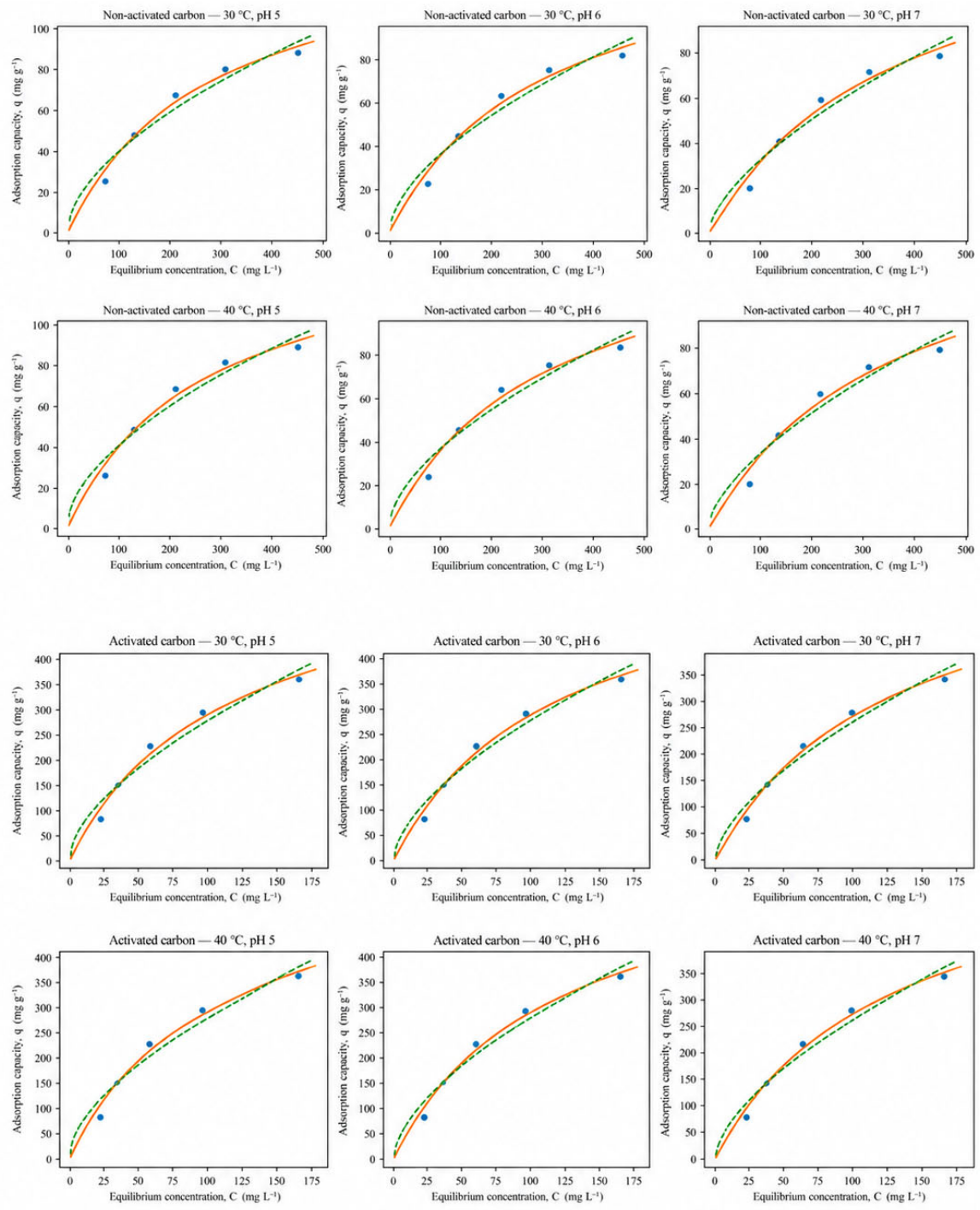


Figure 4. Experimental adsorption isotherms (●) for barley char and activated carbon at 30 °C and 40 °C, with adjustments to the Freundlich (—) and Langmuir (- - -) models.

In this context, the spectral changes observed upon contact with APAP suggest that π–π interactions, n–π interactions, and hydrogen bonding may contribute to the adsorption process [83]. However, these interactions should be considered as possible adsorption mechanisms rather than conclusive evidence, since FTIR alone does not allow their individual contributions to be confirmed. In addition, considering the material's textural properties (Table 2), pore filling may also contribute to the adsorption process [84]. It should be noted that the band at 430 cm^{-1} corresponds to the O–Si–O bending vibration [52], confirming the silicon content reported in Table 1.

This behavior is closely related to the PZC and to the presence of basic functional groups, such as pyrone, chromene, and electron-rich aromatic structures [78]. Since the evaluated materials exhibit PZC values > 7 (Table 3), the adsorbent surfaces acquire a basic character and, within the studied pH range (5–7), remain predominantly positively charged. Under these conditions, APAP (pKa = 9.38) is predominantly present in its neutral form; therefore, electrostatic interactions do not play a significant role in the adsorption process [85]. In this context, hydrogen bonding, π–π interactions, and n–π interactions may contribute to APAP adsorption on the *Hordeum vulgare*-derived activated carbon, as suggested by the observed FTIR shifts. However, these interactions should be considered as possible contributions rather than confirmed dominant adsorption mechanisms.

Table 5 shows the removal efficiency of the *Hordeum vulgare*-derived activated carbon compared to other studies. The removal efficiency decreased from 77.68% at 100 mg L^{-1} to 68.81% at 500 mg L^{-1}. This decrease may be attributed to the limited number of available adsorption sites at a fixed adsorbent dosage, resulting in greater competition for these sites as the initial APAP concentration increased. The results indicate that the removal efficiency remains competitive even at high contaminant loads (500 mg L^{-1}), with values of 30.78% and 17.68% higher than those of Merck commercial activated carbon and jatoba fruit-derived carbon, respectively [47,86].

The decrease in APAP removal efficiency observed as the initial concentration increased from 100 to 500 mg L^{-1} can be attributed to the increasing ratio of APAP molecules to the available adsorption sites on the carbonaceous material. At higher initial concentrations, the adsorption sites are occupied more rapidly, leading to a progressive reduction in the fraction of APAP removed from the aqueous phase. Nevertheless, as shown in Figure 2, the *Hordeum vulgare*-derived carbon exhibited a substantial adsorption capacity under high contaminant-loading conditions. This behavior may be associated with its micro–mesoporous structure, which provides a combination of micropores for efficient adsorption and mesopores that facilitate the diffusion and transport of relatively large organic molecules toward the internal adsorption sites. Consequently, the developed carbon appears particularly suitable for the removal of organic pollutants at relatively high contaminant loads [87].

The removal efficiency may be higher in some cases; however, it depends on the initial contaminant concentration and the adsorbent dose, which are not yet standardized in adsorption studies. In this context, Tran and collaborators [88] used an adsorbent dose of 2 g L^{-1}, whereas Sajid and collaborators [73] employed an initial APAP concentration of 20 mg L^{-1}. Therefore, increasing the adsorbent dose or decreasing the initial contaminant concentration enhances the removal efficiency. However, the comparison in Table 5 should be considered qualitative, since differences in adsorbent dosage, initial concentration, pH, and temperature limit direct comparison among studies. Nevertheless, the results suggest that the *Hordeum vulgare*-derived activated carbon shows promising adsorption performance, supporting the potential valorization of this agricultural residue as an adsorbent material.

Table 5. Comparison with literature reports.

Adsorbent Material	APAP Initial Concentration (mg L^{-1})	Adsorbent Dose (g L^{-1})	Adsorption Capacity (mg g^{-1})	Efficiency (%)	Reference
Hordeum vulgare activated carbon	100	1	74.73	77.68	This study
Hordeum vulgare activated carbon	500	1	363.84	68.81	This study
Merck activated carbon	100	1	83.33	79.00	[47]

Table 5. *Cont.*

Adsorbent Material	APAP Initial Concentration (mg L^{-1})	Adsorbent Dose (g L^{-1})	Adsorption Capacity (mg g^{-1})	Efficiency (%)	Reference
Merck activated carbon	500	1	244.63	46.90	[47]
Pomegranate peel activated carbon	281.5	1	214	76	[89]
Cannabis sativum activated carbon	20	0.12	13.2	40	[74]
Grapefruit peel non-spherical activated carbon	500	2	130	52	[87]
Commercial activated carbon	100–1200	1	221	NR	[75]
Fruits of the jatoba tree activated carbon	500	1	300	60	[86]
Commercial activated carbon WG-15	300	1	129	43	[87]

Note: Adsorption capacities and removal efficiencies are reported under the experimental conditions specified in each study; therefore, direct quantitative comparison among studies should be made with caution because adsorbent dosage, initial concentration, pH, temperature, and contact time differ. NR: Not reported.

4. Conclusions

Hordeum vulgare residues were successfully used as a precursor for activated carbon produced by CO_2 physical activation.

The activation process increased the specific surface area from 23 to 520 m^2 g^{-1} and promoted the development of a micro–mesoporous structure.

The activated carbon reached a highest experimental adsorption capacity (*Qe*) of 363.84 mg g^{-1} for paracetamol, and the equilibrium data were better described by the Freundlich model. These results support the potential valorization of *Hordeum vulgare* residues by converting this low-value agricultural biomass into a value-added adsorbent material for pharmaceutical-contaminated water treatment.

The present study was limited to equilibrium batch experiments using synthetic aqueous solutions. Adsorption kinetics, thermodynamic analysis, regeneration, and performance in real water matrices were not evaluated. These aspects should be addressed in future studies, together with continuous-flow and multicomponent systems, to further evaluate the practical applicability of the developed activated carbon.

Author Contributions: Conceptualization, A.G.C.-C. and C.R.-G.; methodology, A.G.C.-C., C.J.D.-V., C.R.-G. and C.C.-L.; software A.G.C.-C. and C.J.D.-V.; validation, C.R.-G., C.C.-L., O.A.A.-S. and C.A.G.-R. formal analysis, A.G.C.-C., C.R.-G. and C.J.D.-V.; investigation, A.G.C.-C. and C.R.-G.; data curation, A.G.C.-C., C.C.-L. and F.S.-M.; writing—original draft preparation, A.G.C.-C., C.R.-G., C.J.D.-V. and C.C.-L.; and writing—review and editing, A.G.C.-C., C.R.-G., C.C.-L., C.J.D.-V., O.A.A.-S., F.S.-M. and C.A.G.-R.; visualization, A.G.C.-C. and C.R.-G.; supervision, C.R.-G., C.J.D.-V. and C.C.-L.; project administration, C.R.-G., C.C.-L. and O.A.A.-S. All authors have read and agreed to the published version of the manuscript.

Funding: This research received no external funding.

Institutional Review Board Statement: Not applicable.

Informed Consent Statement: Not applicable.

Data Availability Statement: The data presented in this study are available within the article. Additional raw data supporting the findings of this study are available from the corresponding author upon reasonable request.

Acknowledgments: The authors gratefully acknowledge the scholarship No. 1229471 granted by the Secretaría de Ciencia, Humanidades, Tecnología e Innovación (SECIHTI), Mexico, for the doctoral studies of A.G. C.C.

Conflicts of Interest: The authors declare no conflicts of interest.

Abbreviations

The following abbreviations are used in this manuscript:

APAP	Paracetamol
NSAIDs	Non-steroidal anti-inflammatory drugs
BET	Brunauer–Emmett–Teller
DR	Dubinin–Radushkevich
DFT	Density Functional Theory
SEM	Scanning electron microscopy
EDX	Energy-dispersive X-ray spectroscopy
ETD	Secondary electron detectors
BSED	Backscattered electron detectors
FTIR	Fourier-transform infrared spectroscopy
PZC	Point of zero charge
HPLC	High-performance liquid chromatography
Qe	Experimental adsorption capacity
Q_L	Langmuir adsorption capacity
Q_F	Freundlich adsorption capacity
K_L	Langmuir constant
Ce	Equilibrium concentration of the adsorbate in solution
K_F	Freundlich constant
n	Indicator of adsorption intensity
E	Removal efficiency
Ci	Initial APAP concentration
Cf	APAP concentration after 24 h of adsorption
IUPAC	International Union of Pure and Applied Chemistry
pKa	Acid dissociation constant
Q	Adsorption capacity

References

1. Li, X.; Shen, X.; Jiang, W.; Xi, Y.; Li, S. Comprehensive review of emerging contaminants: Detection technologies, environmental impact, and management strategies. *Ecotoxicol. Environ. Saf.* **2024**, *278*, 116420. [CrossRef]
2. Mantovani, M.; Rossi, S.; Ficara, E.; Collina, E.; Marazzi, F.; Lasagni, M.; Mezzanotte, V. Removal of pharmaceutical compounds from the liquid phase of anaerobic sludge in a pilot-scale high-rate alga-bacteria pond. *Sci. Total Environ.* **2023**, *908*, 167881. [CrossRef]
3. Al-Howri, B.M.; Azha, S.F.; Shamsudin, M.S.; Hamid, N.A.; Alsobaai, A.M.; Ismail, S. Paracetamol in diverse water sources: Health hazards and treatment efficacy emphasizing adsorption techniques—A review. *Int. J. Environ. Sci. Technol.* **2024**, *21*, 9743–9762. [CrossRef]
4. Domínguez-García, P.; Fernández-Ruano, L.; Báguena, J.; Cuadros, J.; Gómez-Canela, C. Assessing the pharmaceutical residues as hotspots of the main rivers of Catalonia, Spain. *Environ. Sci. Pollut. Res.* **2024**, *31*, 44080–44095. [CrossRef]
5. Lesser, L.E.; Mora, A.; Moreau, C.; Mahlknecht, J.; Hernández-Antonio, A.; Ramírez, A.I.; Barrios-Piña, H. Survey of 218 organic contaminants in groundwater derived from the world's largest untreated wastewater irrigation system: Mezquital Valley, Mexico. *Chemosphere* **2018**, *198*, 510–521. [CrossRef]
6. Spaltro, A.; Pila, M.N.; Colasurdo, D.D.; Grau, E.N.; Román, G.; Simonetti, S.; Ruiz, D.L. Removal of paracetamol from aqueous solution by activated carbon and silica: Experimental and computational study. *J. Contam. Hydrol.* **2020**, *236*, 103739. [CrossRef]
7. Allegaert, K.; Peeters, M.Y.; Beleyn, B.; Smits, A.; Kulo, A.; Van Calsteren, K.; Deprest, J.; De Hoon, J.; Knibbe, C.A.J. Paracetamol pharmacokinetics and metabolism in young women. *BMC Anesthesiol.* **2015**, *15*, 163. [CrossRef]
8. Fuentes, A.B.; Canevesi, R.; Gadonneix, P.; Mathieu, S.; Celzard, A.; Fierro, V. Paracetamol removal by Kon-Tiki kiln-derived biochar and activated carbons. *Ind. Crops Prod.* **2020**, *155*, 112740. [CrossRef]

9. K'oreje, K.O.; Demeestere, K.; De Wispelaere, P.; Vergeynst, L.; Dewulf, J.; Van Langenhove, H. From multi-residue screening to target analysis of pharmaceuticals in water: Development of a new approach based on magnetic sector mass spectrometry and application in the Nairobi River basin, Kenya. *Sci. Total Environ.* **2012**, *437*, 153–164. [CrossRef]
10. Nödler, K.; Licha, T.; Bester, K.; Sauter, M. Development of a multi-residue analytical method, based on liquid chromatography–tandem mass spectrometry, for the simultaneous determination of 46 micro-contaminants in aqueous samples. *J. Chromatogr.* **2010**, *1217*, 6511–6521. [CrossRef]
11. Lin, A.Y.; Tsai, Y. Occurrence of pharmaceuticals in Taiwan's surface waters: Impact of waste streams from hospitals and pharmaceutical production facilities. *Sci. Total Environ.* **2009**, *407*, 3793–3802. [CrossRef]
12. Gworek, B.; Kijeńska, M.; Zaborowska, M.; Wrzosek, J.; Tokarz, L.; Chmielewski, J. Occurrence of pharmaceuticals in aquatic environment–a review. *Desalin. Water Treat.* **2020**, *184*, 375–387. [CrossRef]
13. Togola, A.; Budzinski, H. Multi-residue analysis of pharmaceutical compounds in aqueous samples. *J. Chromatogr.* **2007**, *1177*, 150–158. [CrossRef]
14. Westerhoff, P.; Yoon, Y.; Snyder, S.; Wert, E. Fate of endocrine-disruptor, pharmaceutical, and personal care product chemicals during simulated drinking water treatment processes. *Environ. Sci. Technol.* **2005**, *39*, 6649–6663. [CrossRef]
15. Pires, P.; Pereira, A.M.P.T.; Pena, A.; Silva, L.J.G. Non-steroidal anti-inflammatory drugs in the aquatic environment and bivalves: The state of the art. *Toxics* **2024**, *12*, 415. [CrossRef]
16. Dewanti, A.I.A.; Kunjirika, T.P.; Putri, R.R.R.D.; Adaninggar, A.; Raharjeng, A.R.P.; Retnoaji, B.; Nuriliani, A.; Sofyantoro, F.; Septriani, N.I.; Saragih, H.T.S.S.G. Effects of paracetamol on the development of zebrafish (*Danio rerio*). *Pertanika J. Trop. Agric. Sci.* **2023**, *46*, 1173–1188. [CrossRef]
17. Gutiérrez-Noya, V.M.; Gómez-Oliván, L.M.; Del Carmen Ramírez-Montero, M.; Islas-Flores, H.; Galar-Martínez, M.; García-Medina, S. Survival and malformations rates, oxidative status in early life stages of *Cyprinus carpio* due to exposure to environmentally realistic concentrations of paracetamol. *Sci. Total Environ.* **2021**, *768*, 144585. [CrossRef]
18. Agarwal, N. Paracetamol—A contaminant of high concern: Existence in environment and adverse effect. *Pharm. Drug Regul. Aff. J.* **2022**, *5*, 000128. [CrossRef]
19. Mangalam, J.; Sharma, J.; Sharma, M.; Mishra, Y.K.; Nigam, S.; Joshi, M. Recent advances of nanomaterials for non-steroidal anti-inflammatory drugs removal from wastewater: A critical review. *Clean Technol. Environ. Policy* **2024**, *26*, 1705–1729. [CrossRef]
20. Lee, W.J.; Goh, P.S.; Lau, W.J.; Ismail, A.F. Removal of pharmaceutical contaminants from aqueous medium: A state-of-the-art review based on paracetamol. *Arab. J. Sci. Eng.* **2020**, *45*, 7109–7135. [CrossRef]
21. Sadegh, F.; Sadegh, N.; Wongniramaikul, W.; Apiratikul, R.; Choodum, A. Adsorption of volatile organic compounds on biochar: A review. *Process Saf. Environ. Prot.* **2024**, *182*, 559–578. [CrossRef]
22. Shen, Y.; Zhou, H.; He, X.; Shen, F.; Xu, Z.; Yang, B.; Kong, L.; Dai, L. Emerging applications of deep eutectic solvents in the preparation and functionalization of biomass-derived carbonaceous materials: Challenges and prospects. *Green Chem.* **2024**, *26*, 8123–8144. [CrossRef]
23. Sanchez-Silva, J.M.; González-Estrada, R.R.; Blancas-Benitez, F.J.; Fonseca-Cantabrana, Á. Utilización de subproductos agroindustriales para la bioadsorción de metales pesados. *TIP Rev. Esp. Cienc. Quím. Biol.* **2020**, *23*, 1–18. [CrossRef]
24. Zgolli, A.; Souissi, M.; Dhaouadi, H. Purification of pesticide-contaminated water using activated carbon from prickly pear seeds for environmentally friendly reuse in a circular economy. *Sustainability* **2024**, *16*, 406. [CrossRef]
25. Kizito, S.; Luo, H.; Lu, J.; Bah, H.; Dong, R.; Wu, S. Role of Nutrient-Enriched Biochar as a Soil Amendment during Maize Growth: Exploring Practical Alternatives to Recycle Agricultural Residuals and to Reduce Chemical Fertilizer Demand. *Sustainability* **2019**, *11*, 3211. [CrossRef]
26. Ruiz, H.; Zambtrano, M.; Giraldo, L.; Sierra, R.; Moreno-Pirajan, J.C. Production and characterization of activated carbon from oil-palm shell for carboxylic acid adsorption. *Orient. J. Chem.* **2015**, *31*, 753–762. [CrossRef]
27. Oickle, A.M.; Goertzen, S.L.; Hopper, K.R.; Abdalla, Y.O.; Andreas, H.A. Standardization of the Boehm titration: Part II. Method of agitation, effect of filtering and dilute titrant. *Carbon* **2010**, *48*, 3313–3322. [CrossRef]
28. Babić, B.; Milonjić, S.; Polovina, M.; Kaludierović, B. Point of zero charge and intrinsic equilibrium constants of activated carbon cloth. *Carbon* **1999**, *37*, 477–481. [CrossRef]
29. Ntakirutimana, S.; Tan, W.; Wang, Y. Enhanced surface activity of activated carbon by surfactants synergism. *RSC Adv.* **2019**, *9*, 26519–26531. [CrossRef]
30. Mukherjee, T.; Rahaman, M. Optimization of acetaminophen adsorption onto biodegradable waste-derived activated carbon using response surface methodology. *Mat. Today Proc.* **2023**, *76*, 233–238. [CrossRef]
31. Gatrouni, M.; Asses, N.; Bedia, J.; Belver, C.; Molina, C.B.; Mzoughi, N. Acetaminophen Adsorption on Carbon Materials from Citrus Waste. *C–J. Carbon Res.* **2024**, *10*, 53. [CrossRef]
32. Hussain, S.; Anjali, K.P.; Hassan, S.T.; Dwivedi, P.B. Waste tea as a novel adsorbent: A review. *Appl. Water Sci.* **2018**, *8*, 165. [CrossRef]

33. Vu, T.M.; Nguyen, T.M.P.; Van, H.; Le, N.T.; Tran, D. Biomass-derived hydrochar and activated carbon in pharmaceutical pollution mitigation: A comprehensive overview. *RSC Adv.* **2025**, *15*, 43053–43084. [CrossRef]
34. Shabir, G.A.; Arain, S.A. Determination of paracetamol, methyl parahydroxybenzoate, ethyl parahydroxybenzoate, and propyl parahydroxybenzoate in medicinal suspension and tablets by RPLC/UV-DAD. *J. Liq. Chromatogr. Relat. Technol.* **2011**, *34*, 719–729. [CrossRef]
35. Vinayagam, R.; Kar, A.; Murugesan, G.; Varadavenkatesan, T.; Goveas, L.C.; Samanth, A.; Ahmed, M.B.; Selvaraj, R. Low temperature carbonized mesoporous graphitic carbon for tetracycline adsorption: Mechanistic insight and adaptive neuro-fuzzy inference system modeling. *Bioresour. Technol. Rep.* **2023**, *22*, 101468. [CrossRef]
36. Wazir, A.H.; Wazir, I.U.; Wazir, A.M. Preparation and characterization of rice husk based physical activated carbon. *Energy Sources Part A Recovery Util. Environ. Eff.* **2024**, *46*, 4875–4885. [CrossRef]
37. Serafin, J.; Dziejarski, B. Activated carbons—Preparation, characterization and their application in CO_2 capture: A review. *Environ. Sci. Pollut. Res.* **2023**, *31*, 40008–40062. [CrossRef]
38. Basta, A.; Fierro, V.; Saied, H.; Celzard, A. Effect of deashing rice straws on their derived activated carbons produced by phosphoric acid activation. *Biom. Bioenerg.* **2011**, *35*, 1954–1959. [CrossRef]
39. Ahmed, M.J.; Anastopoulos, I.; Kalderis, D.; Danish, M. A comprehensive review of barley crop-based materials as adsorbents for the removal of aquatic pollutants. *J. Mol. Liq.* **2024**, *406*, 125151. [CrossRef]
40. Rouquerol, J.; Avnir, D.; Fairbridge, C.W.; Everett, D.H.; Haynes, J.M.; Pernicone, N.; Ramsay, J.D.F.; Sing, K.S.W.; Unger, K.K. Recommendations for the characterization of porous solids (Technical Report). *Pure Appl. Chem.* **1994**, *66*, 1739–1758. [CrossRef]
41. Mays, T. A new classification of pore sizes. *Stud. Surf. Sci. Catal.* **2007**, *160*, 57–62. [CrossRef]
42. Tetteh, I.K.; Issahaku, I.; Tetteh, A.Y. Recent advances in synthesis, characterization, and environmental applications of activated carbons and other carbon derivatives. *Carbon Trends* **2024**, *14*, 100328. [CrossRef]
43. Pietrzak, R. Sawdust pellets from coniferous species as adsorbents for NO_2 removal. *Bioresour. Technol.* **2009**, *101*, 907–913. [CrossRef]
44. Sujiono, E.; Zabrian, D.; Zurnansyah, N.; Mulyati, N.; Zharvan, V.; Samnur, N.; Humairah, N. Fabrication and characterization of coconut shell activated carbon using variation chemical activation for wastewater treatment application. *Results Chem.* **2022**, *4*, 100291. [CrossRef]
45. Neme, I.; Gonfa, G.; Masi, C. Activated carbon from biomass precursors using phosphoric acid: A review. *Heliyon* **2022**, *8*, e11940. [CrossRef]
46. Thommes, M.; Kaneko, K.; Neimark, A.V.; Olivier, J.P.; Rodriguez-Reinoso, F.; Rouquerol, J.; Sing, K.S. Physisorption of gases, with special reference to the evaluation of surface area and pore size distribution (IUPAC Technical Report). *Pure Appl. Chem.* **2015**, *87*, 1051–1069. [CrossRef]
47. Cortés-Cruz, A.G.; Adame-Pereira, M.; Durán-Valle, C.J.; López-Coca, I.M. Hydrothermal modification of activated carbon enhances acetaminophen adsorption: Experimental and computational evidence of π–π interaction dominance. *Molecules* **2025**, *30*, 4295. [CrossRef]
48. Mel'gunov, M.S. Application of the simple Bayesian classifier for the N_2 (77 K) adsorption/desorption hysteresis loop recognition. *Adsorption* **2022**, *29*, 199–208. [CrossRef]
49. Zeng, Y.; Fan, C.; Do, D.D.; Nicholson, D. Evaporation from an ink-bottle pore: Mechanisms of adsorption and desorption. *Ind. Eng. Chem. Res.* **2014**, *53*, 15467–15474. [CrossRef]
50. Coasne, B.; Galarneau, A.; Gerardin, C.; Fajula, F.; Villemot, F. Molecular simulation of adsorption and transport in hierarchical porous materials. *Langmuir* **2013**, *29*, 7864–7875. [CrossRef]
51. McCall, M.A.; Watson, J.S.; Sephton, M.A. Predicting stability of barley straw-derived biochars using Fourier transform infrared spectroscopy. *ACS Sustain. Resour. Manag.* **2024**, *1*, 1975–1983. [CrossRef]
52. Bogeat Barroso, A.; Alexandre-Franco, M.; Fernández-González, C.; Gómez-Serrano, V. Some insights into the evolution of support surface chemistry during the preparation of metal oxide-activated carbon catalysts by conventional wet impregnation. *Bol. Grupo Esp. Carbón* **2021**, *61*, 7–13. Available online: https://gredos.usal.es/handle/10366/167189 (accessed on 1 July 2026).
53. Lilli, B.; Wassersleben, S.; Schulze, T.; Otto, A.; Enke, D. Additive effects of rice husk-based carbon-silica composites on adsorption of diclofenac sodium and carbamazepine from aqueous solutions. *Sci. Total Environ.* **2024**, *954*, 176389. [CrossRef]
54. Charmas, B.; Zięzio, M.; Jedynak, K. Assessment of the porous structure and surface chemistry of activated biocarbons used for methylene blue adsorption. *Molecules* **2023**, *28*, 4922. [CrossRef]
55. Dittmann, D.; Saal, L.; Zietzschmann, F.; Mai, M.; Altmann, K.; Al-Sabbagh, D.; Schumann, P.; Ruhl, A.S.; Jekel, M.; Braun, U. Characterization of activated carbons for water treatment using TGA-FTIR for analysis of oxygen-containing functional groups. *Appl. Water Sci.* **2022**, *12*, 203. [CrossRef]
56. Correa-Abril, J.; Cabrera, E.V.; Robles, N.; Terán, J.L.L.; Stahl, U. Kinetic, equilibrium, and thermodynamic study of Methylene Blue adsorption on orange peel biochar prepared by microwave-assisted pyrolysis. *Sci. Rep.* **2026**, *16*, 8310. [CrossRef]

57. Fidel, R.B.; Laird, D.A.; Thompson, M.L. Evaluation of Modified Boehm Titration Methods for Use with Biochars. *J. Environ. Qual.* **2013**, *42*, 1771–1778. [CrossRef]
58. Bernal, V.; Giraldo, L.; Moreno-Piraján, J.C. Understanding the solid-liquid equilibria between paracetamol and activated carbon: Thermodynamic approach of the interactions adsorbent-adsorbate using equilibrium, kinetic and calorimetry data. *J. Hazard Mater.* **2021**, *419*, 126432. [CrossRef]
59. Mustafa, D.; Ibrahim, B.; Erten, A. Adsorptive removal of anticarcinogen pazopanib from aqueous solutions using activated carbon: Isotherm, kinetic and thermodynamic studies. *Sci. Rep.* **2024**, *14*, 17765. [CrossRef]
60. Oliveira, E.N.; Meneses, A.T.; De Melo, S.F.; Dias, F.M.R.; Perazzini, M.T.B.; Perazzini, H.; Meili, L.; Soletti, J.I.; Carvalho, S.H.V.; Bispo, M.D. Highly effective adsorption of caffeine by a novel activated carbon prepared from coconut leaf. *Environ. Sci. Pollut. Res.* **2022**, *29*, 50661–50674. [CrossRef]
61. Sayğılı, H.; Güzel, F. Effective removal of tetracycline from aqueous solution using activated carbon prepared from tomato (*Lycopersicon esculentum* Mill.) industrial processing waste. *Ecotoxicol. Environ. Saf.* **2016**, *131*, 22–29. [CrossRef]
62. Vinayagam, M.; Babu, R.S.; Sivasamy, A.; De Barros, A.L.F. Impact of carbon dioxide-assisted activation on *Millettia pinnata* shell-derived porous activated carbon for enhanced performance in symmetric supercapacitors. *Ionics* **2024**, *30*, 3045–3054. [CrossRef]
63. Martins, A.C.; Pezoti, O.; Cazetta, A.L.; Bedin, K.C.; Yamazaki, D.A.; Bandoch, G.F.; Asefa, T.; Visentainer, J.V.; Almeida, V.C. Removal of tetracycline by NaOH-activated carbon produced from macadamia nut shells: Kinetic and equilibrium studies. *Chem. Eng. J.* **2014**, *260*, 291–299. [CrossRef]
64. Banik, C.; Lawrinenko, M.; Bakshi, S.; Laird, D.A. Impact of pyrolysis temperature and feedstock on surface charge and functional group chemistry of biochars. *J. Environ. Qual.* **2018**, *47*, 452–461. [CrossRef]
65. Daza Barranco, L.M.; Orrego Mirnda, F.F.; Piñeres Mendoza, J.L.; Fernández Hincapie, J.J. Preparación, caracterización de carbones activados a partir de un carbón mineral de la Cuenca del Cesar (Colombia). *Rev. Politéc.* **2018**, *14*, 75–88. [CrossRef]
66. Angın, D.; Şensöz, S. Effect of pyrolysis temperature on chemical and surface properties of biochar of rapeseed (*Brassica napus* L). *Int. J. Phytoremediation* **2013**, *16*, 684–693. [CrossRef]
67. Vakili, A.; Zinatizadeh, A.; Rahimi, Z.; Zinadini, S.; Mohammadi, P.; Azizi, S.; Karami, A.; Abdulgader, M. The impact of activation temperature and time on the characteristics and performance of agricultural waste-based activated carbons for removing dye and residual COD from wastewater. *J. Clean. Prod.* **2022**, *382*, 134899. [CrossRef]
68. Rajahmundry, G.K.; Garlapati, C.; Kumar, P.S.; Alwi, R.S.; Vo, D.N. Statistical analysis of adsorption isotherm models and its appropriate selection. *Chemosphere* **2021**, *276*, 130176. [CrossRef]
69. Alakayleh, Z. Sulfuric acid-activated carbon from guava leaves for paracetamol adsorption. *Results Eng.* **2024**, *25*, 103685. [CrossRef]
70. Vigdorowitsch, M.; Pchelintsev, A.; Tsygankova, L.; Tanygina, E. Freundlich isotherm: An adsorption model complete framework. *Appl. Sci.* **2021**, *11*, 8078. [CrossRef]
71. Mabalane, K.; Thabede, P.; Shooto, N. Removal of ibuprofen and paracetamol from water using a blend activated carbon from paper waste and avocado seeds. *Green Anal. Chem.* **2024**, *10*, 100135. [CrossRef]
72. Islam, M.A.; Nazal, M.K.; Akinpelu, A.A.; Sajid, M.; Alhussain, N.A.; Ilyas, M. High performance adsorptive removal of emerging contaminant paracetamol using a sustainable biobased mesoporous activated carbon prepared from palm leaves waste. *J. Anal. Appl. Pyrolysis* **2024**, *180*, 106546. [CrossRef]
73. Doczekalska, B.; Kuśmierek, K.; Świątkowski, A. The adsorptive removal of paracetamol as a model pollutant from an aqueous environment using activated carbons made from selected nutshells as agricultural waste. *Processes* **2025**, *13*, 2198. [CrossRef]
74. Sajid, M.; Bari, S.; Rehman, M.S.U.; Ashfaq, M.; Guoliang, Y.; Mustafa, G. Adsorption characteristics of paracetamol removal onto activated carbon prepared from *Cannabis sativum* hemp. *Alex. Eng. J.* **2022**, *61*, 7203–7212. [CrossRef]
75. Nguyen, D.T.; Tran, H.N.; Juang, R.; Dat, N.D.; Tomul, F.; Ivanets, A.; Woo, S.H.; Hosseini-Bandegharaei, A.; Nguyen, V.P.; Chao, H. Adsorption process and mechanism of acetaminophen onto commercial activated carbon. *J. Environ. Chem. Eng.* **2020**, *8*, 104408. [CrossRef]
76. Hashemzadeh, F.; Ariannezhad, M.; Derakhshandeh, S.H. Sustainable removal of tetracycline and paracetamol from water using magnetic activated carbon derived from pine fruit waste. *Sci. Rep.* **2024**, *14*, 16346. [CrossRef]
77. Bouzidi, M.; Sellaoui, L.; Mohamed, M.; Franco, D.S.P.; Erto, A.; Badawi, M. A comprehensive study on paracetamol and ibuprofen adsorption onto biomass-derived activated carbon through experimental and theoretical assessments. *J. Mol. Liq.* **2023**, *376*, 121457. [CrossRef]
78. Mokhtaryan, S.; Khodabakhshi, A.; Sadeghi, R.; Nourmoradi, H.; Shakeri, K.; Hemati, S.; Mohammadi-Moghadam, F. New activated carbon derived from *Gundelia tournefortii* seeds for effective removal of acetaminophen from aqueous solutions: Adsorption performance. *Arab. J. Chem.* **2023**, *16*, 105253. [CrossRef]
79. Pauletto, P.S.; Lütke, S.F.; Dotto, G.L.; Salau, N.P.G. Adsorption mechanisms of single and simultaneous removal of pharmaceutical compounds onto activated carbon: Isotherm and thermodynamic modeling. *J. Mol. Liq.* **2021**, *336*, 116203. [CrossRef]

80. Zapata, F.; López-Fernández, A.; Ortega-Ojeda, F.; Quintanilla, G.; García-Ruiz, C.; Montalvo, G. Introducing ATR-FTIR spectroscopy through analysis of acetaminophen drugs: Practical lessons for interdisciplinary and progressive learning for undergraduate students. *J. Chem. Educ.* **2021**, *98*, 2675–2686. [CrossRef]
81. Walczak, R.; Savateev, A.; Heske, J.; Tarakina, N.V.; Sahoo, S.; Epping, J.D.; Kühne, T.D.; Kurpil, B.; Antonietti, M.; Oschatz, M. Controlling the strength of interaction between carbon dioxide and nitrogen-rich carbon materials by molecular design. *Sustain. Energy Fuels* **2019**, *3*, 2819–2827. [CrossRef]
82. Ninh, P.T.T.; Tuyen, L.T.N.; Dat, N.D.; Nguyen, M.L.; Dong, N.T.; Chao, H.; Tran, H.N. Two-stage preparation of highly mesoporous carbon for super-adsorption of paracetamol and tetracycline in water: Important contribution of pore filling and π-π interaction. *Environ. Res.* **2022**, *218*, 114927. [CrossRef]
83. Mahmoud, R.; Mahgoub, S.M.; Ashraf, A.M.; Allam, A.A.; Alawam, A.S.; Rudayni, H.A.; Moaty, S.A. Activated carbon alginate as adsorbent for simultaneous removal of almotriptan and paracetamol from binary solutions. *Sustain. Chem. Pharm.* **2024**, *41*, 101708. [CrossRef]
84. Islam, M.A.; Nazal, M.K.; Sajid, M.; Suliman, M.A. Adsorptive removal of paracetamol from aqueous media: A review of adsorbent materials, adsorption mechanisms, advancements, and future perspectives. *J. Mol. Liq.* **2024**, *396*, 123976. [CrossRef]
85. Villaescusa, I.; Fiol, N.; Poch, J.; Bianchi, A.; Bazzicalupi, C. Mechanism of paracetamol removal by vegetable wastes: The contribution of π–π interactions, hydrogen bonding and hydrophobic effect. *Desalination* **2010**, *270*, 135–142. [CrossRef]
86. Spessato, L.; Bedin, K.C.; Cazetta, A.L.; Souza, I.P.; Duarte, V.A.; Crespo, L.H.; Silva, M.C.; Pontes, R.M.; Almeida, V.C. KOH-super activated carbon from biomass waste: Insights into the paracetamol adsorption mechanism and thermal regeneration cycles. *J. Hazard. Mater.* **2019**, *371*, 499–505. [CrossRef]
87. Jedynak, K.; Szczepanik, B.; Rędzia, N.; Słomkiewicz, P.; Kolbus, A.; Rogala, P. Ordered mesoporous carbons for adsorption of paracetamol and non-steroidal anti-inflammatory drugs: Ibuprofen and naproxen from aqueous solutions. *Water* **2019**, *11*, 1099. [CrossRef]
88. Tran, H.N.; Tomul, F.; Ha, N.T.H.; Nguyen, D.T.; Lima, E.C.; Le, G.T.; Chang, C.; Masindi, V.; Woo, S.H. Innovative spherical biochar for pharmaceutical removal from water: Insight into adsorption mechanism. *J. Hazard. Mater.* **2020**, *394*, 122255. [CrossRef]
89. Solmaz, A.; Sari, Z.A.; Karta, M.; Turna, T.; Yücel, A.; Depci, T. Production and Characterization of Activated Carbon from Pomegranate Peel for Pharmaceutical Waste (Paracetamol) Removal: Response Surface Methodology Application. *Water Air Soil Pollut.* **2023**, *234*, 645. [CrossRef]

Disclaimer/Publisher's Note: The statements, opinions and data contained in all publications are solely those of the individual author(s) and contributor(s) and not of MDPI and/or the editor(s). MDPI and/or the editor(s) disclaim responsibility for any injury to people or property resulting from any ideas, methods, instructions or products referred to in the content.